EPR and differential-scanning-calorimetric measurements in Mn^{2+}-doped $ZnZrF_6 \cdot 6H_2O$ and $CoZrF_6 \cdot 6H_2O$

Geetha Jayaram and V. G. Krishnan
Physics Department, Osmania University, Hyderabad 500 007, India
(Received 2 March 1993; revised manuscript received 15 September 1993)

Electron-paramagnetic-resonance (EPR) spectra recorded for Mn^{2+}-doped $ZnZrF_6 \cdot 6H_2O$ and $CoZrF_6 \cdot 6H_2O$ show the presence of "forbidden transitions" $\Delta m_I = \pm 1, \pm 2$ for the central fine-structure transition and $\Delta m_I = \pm 1$ for the remaining fine-structure transitions in the case of the zinc lattice and $\Delta m_I = \pm 1$ again for the central fine transition for the cobalt lattice. At elevated temperatures, a phase transition indicated by differential-scanning-calorimetry does not appear in the EPR spectra, possibly due to a change in the space group but not the point symmetry at the Mn^{2+} ion site. The doublet separations for forbidden transitions are accounted for by using third-order perturbation theory invoking a quadrupole interaction, $Q' = 0.5$ G. The Mn^{2+} spectra in the cobalt lattice are characterized by (a) large linewidths that decrease with increasing temperature and broaden out at low temperatures, (b) an anomalous intensity distribution among the fine-structure lines, and (c) a marked positive g shift, all of which are attributed to the Co-Mn interaction.

INTRODUCTION

$ZnSiF_6 \cdot 6H_2O$ was the first of the series $M^{II}M^{IV}F_6 \cdot 6H_2O$ (M^{II}=Mg, Zn, Co, Ni, Fe, M^{IV}=Si, Ti, Sn) studied by electron-paramagnetic resonance (EPR) using Mn^{2+} ions as a probe.[1] Subsequently a large number of studies have appeared in which Mn^{2+} ions were used to investigate the phase transition form the high-symmetry trigonal unit cell to a low-symmetry monoclinic unit cell.[2–7] A common observation was a spectrum consisting of five groups of six lines in accordance with the selection rules $\Delta M_s = \pm 1$, $\Delta m_I = 0$. Bleaney and Ingram[1] observed a number of weak lines when the external field was along an arbitrary direction. Subsequently, Friedman and Low[2] studied these and assigned them as the "forbidden" transitions obeying the selection rules $\Delta M_s = \pm 1$, $\Delta m_I = \pm 1$ within the central sextet. Bleaney and Rubins[8] observed $\Delta m_I = \pm 2$ transitions, in addition to the $\Delta m_I = \pm 1$, and developed the theory for the angular dependence of these lines. The lines arise from an admixture of spin states due to off-diagonal terms in the Hamiltonian when the magnetic field is not directed along a principal magnetic axis or more specifically the rotation axis of the D tensor.

One of the authors has studied the phase transitions using the EPR spectra of Mn^{2+} ions in a number of compounds of the series, viz., $CoSiF_6 \cdot 6H_2O$,[9] $ZnTiF_6 \cdot 6H_2O$,[10] (Cd,Cd,Fe)$TiF_6 \cdot 6H_2O$,[11] and (Cd,Co,Fe)$SiF_6 \cdot 6H_2O$,[12] (Co,Fe)$SnF_6 \cdot 6H_2O$.[12] Ziatdinov *et al.*[13] have reported the absence of any phase transition in $ZnZrF_6 \cdot 6H_2O$ at low temperatures. Phase transitions in all these $M^{II}M^{IV}F_6 \cdot 6H_2O$ compounds have been attributed to the hindering of the rotation of the ME_6^{2-} octahedron. The absence of a phase transition at low temperatures would therefore lead to the formation of a stable O—H $\cdots$ F bond, which in turn would result in a nonfluctuating electric-field gradient (EFG) at the paramagnetic metal-ion site. Such an effect would lead to a contribution to the quadrupole term. However, at high temperatures such a rotation of the MF_6^{2-} octahedron could be initiated as was reported for $CaSnCl_6 \cdot 6H_2O$.[14]

Further, the paramagnetic host Co^{2+} ion completely surrounds the Mn^{2+} impurity ion. Therefore the dominant contribution to the second moment arises from the dipolar interaction between these two ions. The effective spin-lattice relaxation time for Mn^{2+} is shortened owing to the coupling with the rapidly fluctuating fields produced by the host ions. This effect is known to result in increased linewidths. The anomalous intensities among the fine-structure lines and the marked g shift are the other features that have been reported. The cobalt lattice was studied with a view to check the above features.

Here we report in detail a study of Mn^{2+} EPR spectra in single crystals of $ZnZrF_6 \cdot 6H_2O$ and $CoZrF_6 \cdot 6H_2O$ in the temperature range 153–410 K and 153–393 K, respectively. The choice of these crystals was made with the intention of carrying out a detailed investigation and analysis of the forbidden transitions which were present in all the fine-structure sets. Apart from this, the existence of a possible phase transition from a trigonal to a high-temperature cubic phase was also of interest. This has to the best of our knowledge hitherto not been reported for this type of compound.

EXPERIMENTAL AND STRUCTURAL DETAILS

Single crystals of $ZnZrF_6 \cdot 6H_2O$ and $CoZrF_6 \cdot 6H_2O$ were grown from highly acidic equimolar solutions of ZnF_2/CoF_2 with ZrF_4 at ambient temperature. The crystals grew as hexagonal rods and the impurity content was less than 100 ppm.

The point-symmetry group of $Zn(H_2O)_6$ complex in $ZnZrF_6 \cdot 6H_2O$ (Refs. 15 and 16) is S_6 (the symmetry group of the crystal is $R\bar{3}$ for $Z=1$). Detailed x-ray

0163-1829/94/49(18)/12813(10)/$06.00

studies of $ZnZrF_6 \cdot 6H_2O$ and $CoZrF_6 \cdot 6H_2O$ have not been carried out. However, we have recorded the powder x-ray-diffraction patterns and verified that the Zn and Co lattices are isostructural and belong to the trigonal class of crystals.

EPR spectra were recorded on a conventional x-band spectrometer (JEOL JES-RE3X) with a 12-in. magnet and 100-kHz magnetic-field modulation along with the JEOL low-temperature accessory. With such an accessory, the lowest temperature that could be reached was 153 K.

THEORY

EPR spectra of Mn^{2+} ions in sites of trigonal symmetry have been investigated and the theory well developed. The spectra can be fitted with the following spin Hamiltonian:

$$\mathcal{H}=g\beta H+D[S_z^2-(1/3)S(S+1)]+(1/6)a[(S_\alpha^4+S_\beta^4+S_\gamma^4)-(1/5)S(S+1)(3S^2+S-1)] +(1/180)F[35S_z^4-30S(S+1)S_z^2+25S_z^2-6S(S+1)+3S^2(S+1)]+A\,\text{S.I.}\ , \quad (1)$$

where S_α, S_β, and S_γ are the spin operators with respect to the cube axes and a, D, and F are the zero-field splitting (ZFS) parameters due to the cubic and axial crystalline fields, respectively. These three terms give rise to the fine-structure lines in the spectrum. A is the hyperfine coupling constant. To determine the positions of the fine-structure lines when the field is at some arbitrary angle θ to the trigonal axis, the coordinate system of the molecule is rotated by an angle θ about the y axis and the S_z' of the new coordinate system expressed in terms of the S_z of the original coordinate system. The resultant spin-Hamiltonian is then applied to the spin eigenstates and the off-diagonal terms neglected to give the energies to first order in D. The energies are then corrected to second order by means of nondegenerate perturbation theory. The resulting[17] equations when $\theta=0$ and $p=-2/3$ reduce to

$$m_s \pm 5/2 \leftrightarrow \pm 3/2\ , \quad H=H_0 \pm [4D-(4/3)(a-F)]\ , \quad (2)$$

$$m_s \pm 3/2 \leftrightarrow \pm 1/2\ , \quad H=H_0 \pm [2D+(5/3)(a-F)]\ , \quad (3)$$

$$m_s+1/2 \leftrightarrow -1/2\ , \quad H=H_0\ . \quad (4)$$

If the fine-structure line separations are experimentally determined, the parameters can be evaluated. At $\theta=0$ and 90°, however, the a and F terms cannot be separated. They can be separated at intermediate angles but this requires a knowledge of p at these angles. In most cases F is considered small compared to a and $(a-F)$ is approximated as a. For trigonal crystals such as $ZnZrF_6 \cdot 6H_2O$ and $CoZrF_6 \cdot 6H_2O$, some overlap of lines due to relatively small ZFS is seen. The five fine-structure lines are arranged symmetrically around the central $-\frac{1}{2}$ to $+\frac{1}{2}$ line. The separation between the $\pm\frac{5}{2} \leftrightarrow \pm\frac{3}{2}$ and the $\pm\frac{3}{2} \leftrightarrow \pm\frac{1}{2}$ transitions is $2D-3(a-F)$, while the separation between $\pm\frac{3}{2} \leftrightarrow \pm\frac{1}{2}$ and the $-\frac{1}{2}$ to $+\frac{1}{2}$ transitions is $2D+(\frac{5}{3})(a-F)$. The absolute sign of D and $(a-F)$, however, cannot be determined from the fine-structure line positions alone. If the hyperfine term from the spin-Hamiltonian is included, a term

$$-Am_I-(B^2/2H_0)[\tfrac{35}{4}-m_I^2+m_I(2M_s-1)]$$

must be added to the expressions for the fine-structure lines when H is parallel to the threefold axis. Hence the hyperfine line separation will not be constant but will vary with changing field due to the second-order terms in B. The separation between the $m_I-\frac{5}{2} \leftrightarrow -\frac{5}{2}$ and $m_I\frac{5}{2} \leftrightarrow \frac{5}{2}$ transitions is $-5A-(5B^2/2H_0)(2M_s-1)$.

If A is assumed negative, as is always the case for Mn^{2+} ion, then the above separation will be largest for small values of M_s. Referring to Eqs. (2)–(4) it is obvious that low M_s values occur at high fields for positive D and low fields for negative D. Thus, if the hyperfine splitting increases with increasing field, D is positive and vice versa.

The following procedure was adopted to determine the forbidden hyperfine doublet separation within the hyperfine (hf) sextet corresponding to all five fine-structure transitions.

If the external magnetic field H makes an angle θ with the z axis (the principal axis of the D tensor or the C_3 axis) the Hamiltonian [Eq. (1)] can be written as

$$\mathcal{H}=g\beta HS_z+\sigma\{S_z^2-(1/3)S(S+1)\}+\rho S_+^2+\rho S_-^2 +(\lambda/2)(S_zS_++S_+S_z)+(\lambda/2)(S_zS_-+S_-S_z) +AS_zI_z+(B/2)(S_+I_-+S_-I_+)-\gamma\beta_N HI_z -P\{I_z^2-(1/3)I(I+1)\}\ . \quad (5)$$

Here,

$$S_+=S_x+iS_y\ , \quad S_-=S_x-iS_y\ ,$$

$$\sigma=(1/2)[D(3\cos^2\theta-1)]\ ,$$

$$\rho=(1/4)[D\sin^2\theta]\ ,$$

$$\lambda=D\sin\theta\cos\theta\ ,$$

$$P=(1/2)[Q'(3\cos^2\theta-1)]\ .$$

In the above, a small anisotropy in the hyperfine constant and g value are neglected for simplicity. The eigenvalues of the above Hamiltonian, with z as the axis of quantization and under the approximation $g\beta H \gg |D|, |A|$, are given to third-order of perturbation theory by Schneider and Sircar,[18] Waldner,[19] Takeda,[20] and DeWijn and van Balderen.[21] The forbidden doublet separations in all the five fine structure transitions are given in the Appendix.

TABLE I. Spin-Hamiltonian parameters for $ZnM^{IV}F_6 \cdot 6H_2O$ type of compounds (M^{IV}=Zr, Ti, Ge, Si, and NbO).

System	g	D (G)	$(a-F)$ (G)	A (G)	Ref.
$ZnZrF_6 \cdot 6H_2O$	1.996	−180	−5.0	−93.7	This work
	+0.002	+2		+	
$ZnZrF_6 \cdot 6H_2O$	2.000	−162	−6.4	−97.5	16
$ZnTiF_6 \cdot 6H_2O$	2.003	−185	−7.8	−92.5	11
$ZnGeF_6 \cdot 6H_2O$	2.001	−191	−8.0	−95.0	22
$ZnSiF_6 \cdot 6H_2O$	2.000	−191	−7.5	−95.0	23
$ZnNbOF_5 \cdot 6H_2O$	2.003	−168.8	−9.0	−89.0	24

RESULTS

A. Angular variation

1. $ZnZrF_6 \cdot 6H_2O$

For H along the c axis the spectrum showed a single set of 30 lines, consistent with the crystal structure, with the maximum spread [Fig. 1(a)]. Figure 1(b) shows the spectrum recorded with H making an angle of 10° with the c axis. The forbidden transitions ($\Delta m_I = \pm 1$) are indicated above. Further rotation by 10° results in a spectrum that clearly shows not only the $\Delta m_I = \pm 2$ for the central sextet but $\Delta m_I = \pm 1$ for the other four hyperfine sextets also. The spectrum recorded for H perpendicular to the c axis was invariant under rotation and is shown in Fig. 1(c). Figure 2 shows the angular variation of the hyperfine as well as the fine-structure line positions from $H \| c$ to $H \perp c$. The theoretically predicted ($3\cos^2\theta - 1$) variation for the fine-structure line positions may be seen. The fine-structure line positions were calculated using Eqs. (2)–(4). The hyperfine separation among the five sextets was found to decrease with increasing field. Therefore the sign of D was taken to be negative. Table I shows the

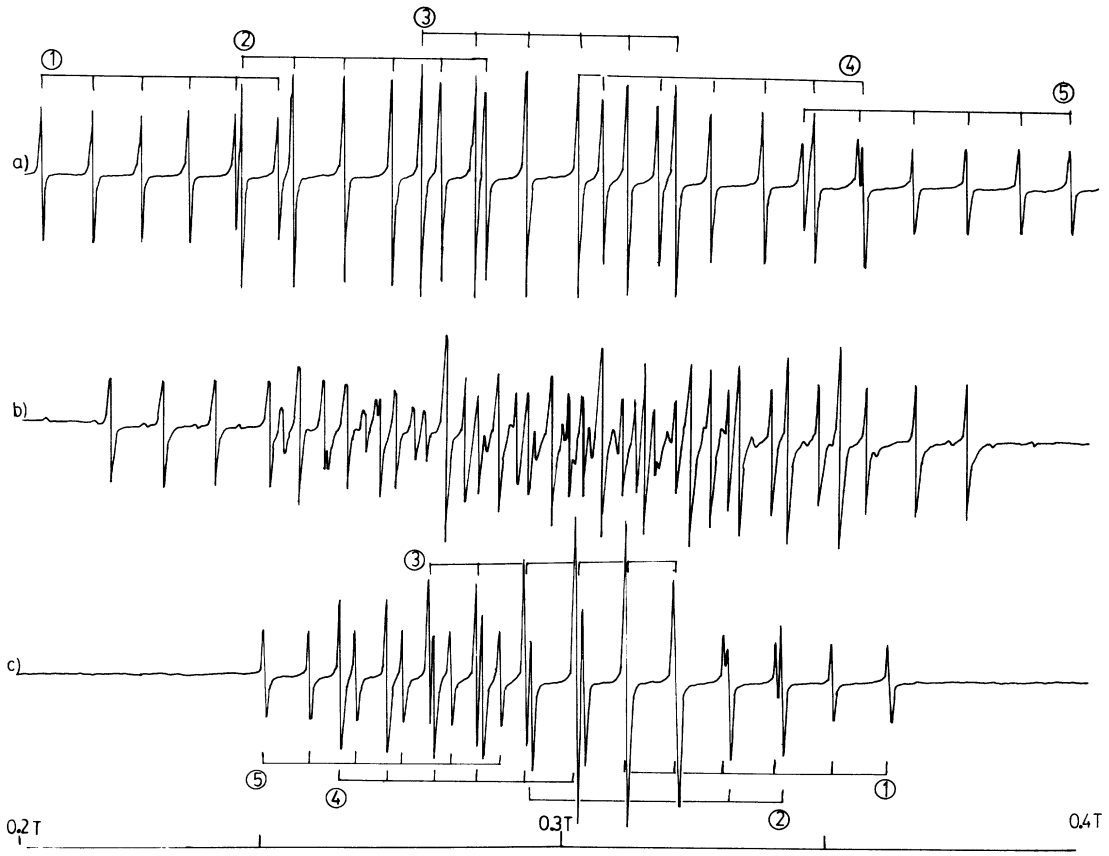

FIG. 1. Room-temperature EPR spectra of Mn^{2+}:$ZnZrF_6 \cdot 6H_2O$ with H (a) along c axis, (b) making an angle of 10° with c axis, (c) perpendicular to c axis (ν=9.246 GHz). Assignment of fine-structure transitions: (1) $-\frac{5}{2} \leftrightarrow -\frac{3}{2}$, (2) $-\frac{3}{2} \leftrightarrow -\frac{1}{2}$, (3) $-\frac{1}{2} \leftrightarrow +\frac{1}{2}$, (4) $+\frac{1}{2} \leftrightarrow \frac{3}{2}$, and (5) $+\frac{3}{2} \leftrightarrow \frac{5}{2}$.

TABLE II. Spin-Hamiltonian parameters for $CoM^{IV}F_6 \cdot 6H_2O$ type of compounds (M^{IV}=Zr, Si, Sn, Ti).

System	D (G)	g	$(a-F)$ (G)	A (G)	Ref.
$CoZrF_6 \cdot 6H_2O$	−181	2.023	−5.2	−92.3	This work
$CoSiF_6 \cdot 6H_2O$	−185	2.0095	−7.4	−95.0	9
	−191	2.001	−2.6	−99.5	6
$CoSnF_6 \cdot 6H_2O$	−192	2.005	−7.8	−92.0	12
	−205	2.0014	2.6	−98.5	6
$CoTiF_6 \cdot 6H_2O$	−195	2.008	−9.4	−93.1	11
$CoNbOF_5 \cdot 6H_2O$	−176	2.0095	−14.0	−88.0	24
$CoPtCl_6 \cdot 6H_2O$	−167	2.0012	−3.0	−97.5	6

spin-Hamiltonian parameters for $ZnZrF_6 \cdot 6H_2O$ along with those of $ZnTiF_6 \cdot 6H_2O$, $ZnGeF_6 \cdot 6H_2O$, $ZnSiF_6 \cdot 6H_2O$, and $ZnNbOF_5 \cdot 6H_2O$.

2. $CoZrF_6 \cdot 6H_2O$

The spectrum along c axis [Fig. 3(a)] shows the expected five sextets for a single-site occupancy in a trigonal unit cell. The intensity of the hyperfine sextets showed considerable deviation from the theoretically predicted values of 5:8:9:8:5. The ZFS is evaluated using the spectrum along the c axis. The spectrum was invariant for rotation about c axis. Figure 3(b) shows this spectrum. The sign of the ZFS parameter was evaluated using the second-order effects in the hyperfine splittings as in the zinc analog. Figure 4 shows the angular variation from $H \| c$ to $H \perp c$, with the H plane containing the c axis. The linewidth varied from 11 G for the low-field sextet to 16 G for the high-field sextet. Table II shows the spin-Hamiltonian parameters for $CoZrF_6 \cdot 6H_2O$ along with those of $CoSiF_6 \cdot 6H_2O$, $CoTiF_6 \cdot 6H_2O$, $CoSnF_6 \cdot 6H_2O$, $CoNbOF_5 \cdot 6H_2O$, and $CoPtF_6 \cdot 6H_2O$ with similar structures.

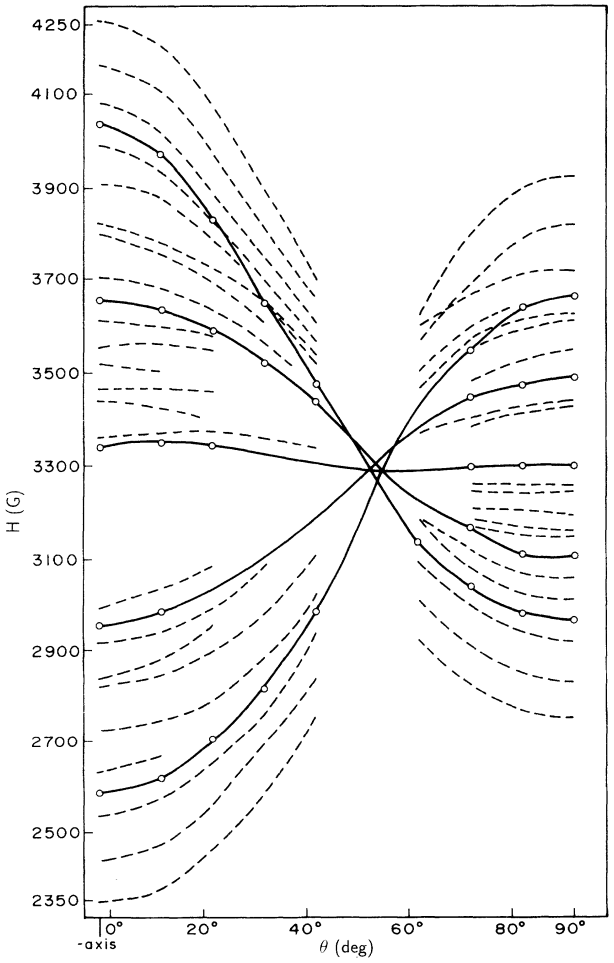

FIG. 2. Angular variation of hyperfine lines (— — —) and fine-structure (○--○) for θ=0° (c axis) to θ=90° (perpendicular to c axis) for Mn^{2+}:$ZnZrF_6 \cdot 6H_2O$.

B. Forbidden hyperfine lines

1. $ZnZrF_6 \cdot 6H_2O$

The forbidden transitions seen in the spectrum [Fig. 1(b)] have been analyzed using Eqs. (A1)–(A6) in the Appendix. The observed doublet separation for forbidden transitions ($\Delta m_I = \pm 1, \pm 2$) were accounted for by using third-order perturbation theory and invoking a quadrupole interaction with $Q' = 0.5 \pm 0.05$ G. The observed and calculated values are given in Tables III–VIII. The value of Q' is chosen to achieve a satisfactory agreement with the observed separation.

TABLE III. Observed and calculated doublet separations of forbidden transitions in Mn^{2+}:$ZnZrF_6 \cdot 6H_2O$. For $\Delta m_I = \pm 1$ in the $M_s = -\frac{1}{2} \leftrightarrow +\frac{1}{2}$ fine-structure transition (ν=9.246 GHz, T=295 K, θ=10).

	$H_{\|-1/2,m_I\rangle \leftrightarrow \|+1/2,m_I+1\rangle} - H_{\|-1/2,m_I+1\rangle \leftrightarrow \|+1/2,m_I\rangle}$	
m_I	Expt. (G)	Theor. (G)
$-\frac{5}{2}$	19.0	19.3
$-\frac{3}{2}$	21.9	22.2
$-\frac{1}{2}$	24.3	25.0
$+\frac{1}{2}$	28.5	27.9
$+\frac{3}{2}$	32.0	30.7

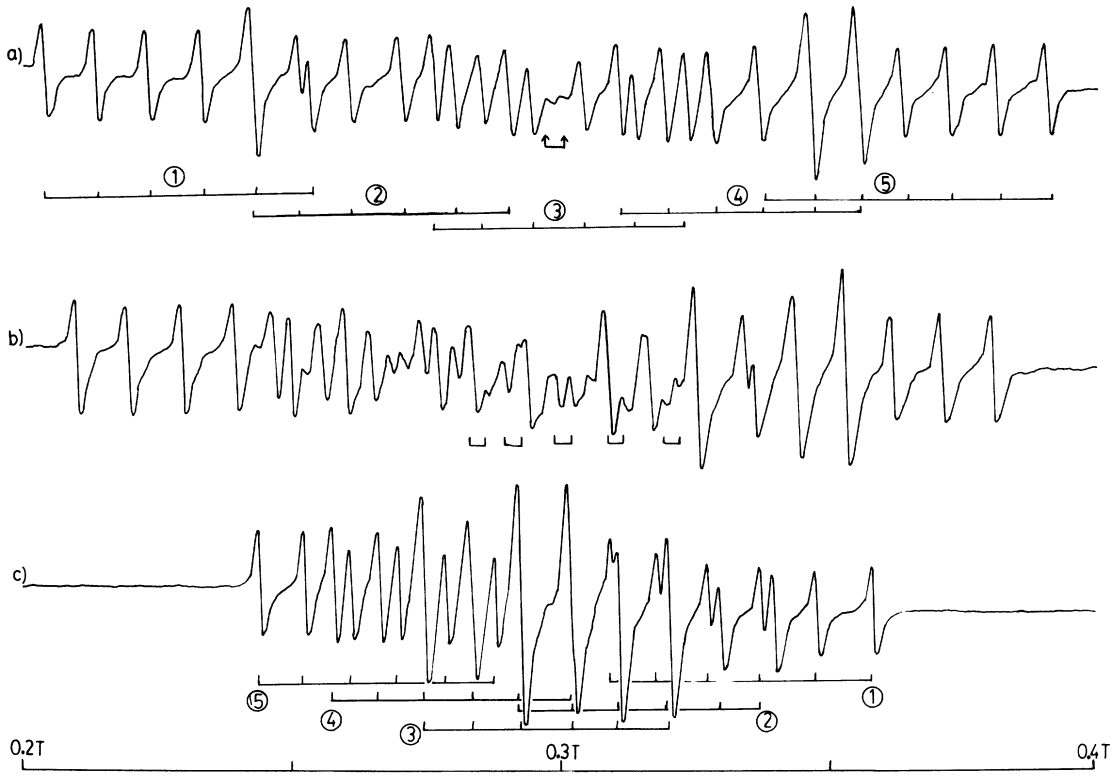

FIG. 3. Room-temperature EPR spectra of Mn^{2+}:$CoZrF_6 \cdot 6H_2O$ with H (a) along c axis, (b) making an angle of 10° with c axis, (c) perpendicular to c axis ($\nu = 9.246$ GHz). Assignment of fine-structure transitions: (1) $-\frac{5}{2} \leftrightarrow -\frac{3}{2}$, (2) $-\frac{3}{2} \leftrightarrow -\frac{1}{2}$, (3) $-\frac{1}{2} \leftrightarrow +\frac{1}{2}$, (4) $+\frac{1}{2} \leftrightarrow +\frac{3}{2}$, and (5) $+\frac{3}{2} \leftrightarrow \frac{5}{2}$.

2. $CoZrF_6 \cdot 6H_2O$

Figure 3(a) shows a pair of forbidden hyperfine lines corresponding to $m_I = +(\frac{1}{2})$. When the c axis is rotated 10° from the H direction, five pairs of forbidden transitions are seen [Fig. 3(b)], for the central sextet only. From the observations in $ZnZrF_6 \cdot 6H_2O$ and the close similarity of the two crystals, as seen from their ZFS parameters, it is possible to say that the forbidden transitions for the remaining four hyperfine sextets are masked primarily by the large linewidths. Table IX gives the forbidden doublet separation for the central sextet calculated using Eq. (A1) along with the observed values. As in $ZnZrF_6 \cdot 6H_2O$ the major contribution to the forbidden transitions is due to the D term with additional contributions from the quadrupole term Q'. This in turn is due to the EFG at the Mn^{2+} site from the rigid O—H · · · F hydrogen bonds.

C. Variable temperature studies and phase transitions

1. $ZnZrF_6 \cdot 6H_2O$

Differential scanning calorimetry (DSC) studies show that the phase transitions occur at $T/K = 370$ and 400.6, involving energies of 200.4 J/gm and 229.2 J/gm, respectively. In order to study these transitions EPR spectra are recorded at $T/K = 363$, 383, and 413. The spectra showed a marked reduction in intensity with increase in temperature. The outer sextets became too weak to be

TABLE IV. Observed and calculated doublet separations of forbidden transitions in Mn^{2+}:$ZnZrF_6 \cdot 6H_2O$. For $\Delta m_I = \pm 2$ in the $M_s = -\frac{1}{2} \leftrightarrow +\frac{1}{2}$ fine-structure transition.

m_I	$H_{\lvert -1/2, m_I - 1\rangle \leftrightarrow \lvert +1/2, m_I + 1\rangle} - H_{\lvert -1/2, m_I + 1\rangle \leftrightarrow \lvert +1/2, m_I\rangle}$ Expt. (G)	Theor. (G)
$-\frac{3}{2}$	39.0	37.9
$-\frac{1}{2}$	31.0	29.6
$+\frac{1}{2}$	26.5	25.3
$+\frac{3}{2}$	22.5	21.2

TABLE V. Observed and calculated doublet separations of forbidden transitions in Mn^{2+}:$ZnZrF_6 \cdot 6H_2O$. For $\Delta m = \pm 1$ in the $M_s = -\frac{3}{2} \leftrightarrow -\frac{1}{2}$ fine-structure transition.

m_I	$H_{\lvert -1/2, m_I\rangle \leftrightarrow \lvert -3/2, m_I + 1\rangle} - H_{\lvert -1/2, m_I + 1\rangle \leftrightarrow \lvert -3/2, m_I\rangle}$ Expt. (G)	Theor. (G)
$-\frac{5}{2}$	159.5	156.7
$-\frac{3}{2}$	162.2	160.3
$-\frac{1}{2}$	166.4	164.3
$+\frac{1}{2}$	171.6	170.6
$+\frac{3}{2}$	173.9	172.5

observed leaving behind only the central sextet. The linewidths, however, remained nearly unchanged. Figure 5 shows the variation of ZFS with temperature along with that of $CoZrF_6 \cdot 6H_2O$. The increase in D with temperature, though small, is similar for both the lattices.

2. $CoZrF_6 \cdot 6H_2O$

The DSC study for this compound also showed the onset of a phase transition at $T/K = 343.7$ and completion at 375.4, involving an energy of 197.9 J/gm. EPR spectra of Mn^{2+} in $CoZrF_6 \cdot 6H_2O$ at room temperature showed hf lines with widths ~ 11 G, which are larger than the 4 G in $ZnZrF_6 \cdot 6H_2O$. EPR spectra are recorded at $T/K = 313$, 333, 343, 353, 368, 377, 387, and 397. The lines were seen to narrow down with increasing temperature, reaching about 8 G at the highest temperature. The intensity was seen to be nearly constant, except for the highest two temperatures, where there was a slight decrease. Above 363 K there was a gradual reduction in the spread. The lines broaden on lowering the temperature, disappearing completely at $T/K = 153$. Figure 6 shows the spectrum along c axis at $T/K = 183$.

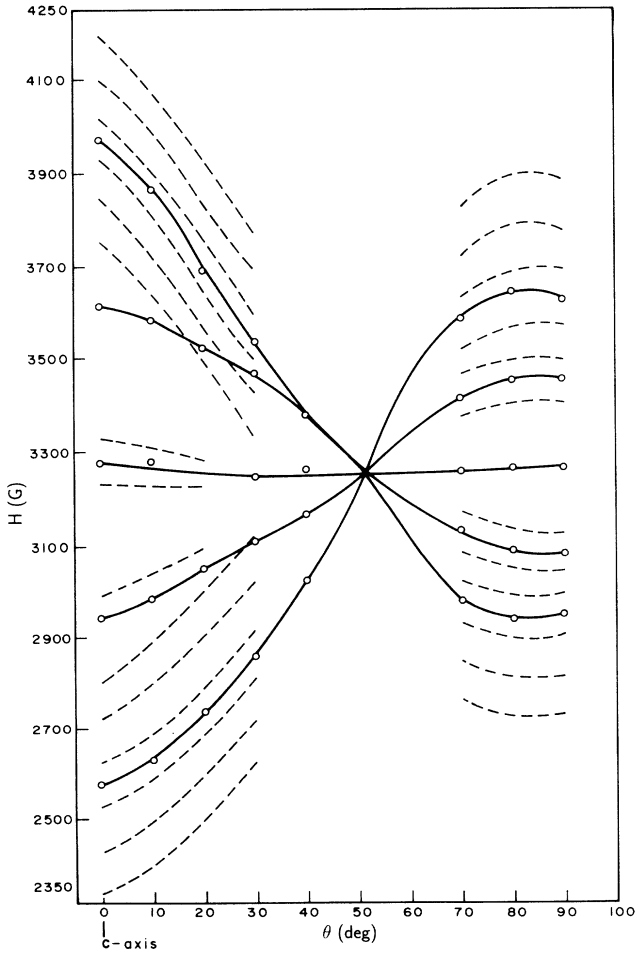

FIG. 4. Angular variation of hyperfine lines (— — —) and fine-structure (○--○) for $\theta = 0°$ (c axis) to $\theta = 90°$ (perpendicular to c axis) for Mn^{2+}:$CoZrF_6 \cdot 6H_2O$.

TABLE VI. Observed and calculated doublet separations of forbidden transitions in Mn^{2+}:$ZnZrF_6 \cdot 6H_2O$. For $\Delta m_I = \pm 1$ in the $M_s = -\frac{5}{2} \leftrightarrow \frac{3}{2}$ fine-structure transition.

	$H_{\lvert -5/2, m_I \rangle \leftrightarrow \lvert -3/2, m_I+1 \rangle} - H_{\lvert -5/2, m_I+1 \rangle \leftrightarrow \lvert -3/2, m_I \rangle}$	
m_I	Expt. (G)	Theor. (G)
$-\frac{5}{2}$	333.4	330.6
$-\frac{3}{2}$	342.7	340.5
$-\frac{1}{2}$	351.9	350.6
$+\frac{1}{2}$	364.0	361.1
$+\frac{3}{2}$	373.0	371.8

TABLE VII. Observed and calculated doublet separations of forbidden transitions in Mn^{2+}:$ZnZrF_6 \cdot 6H_2O$. For $\Delta m_I = \pm 1$ in the $M_s = +\frac{1}{2} \leftrightarrow +\frac{3}{2}$ fine-structure transition.

	$H_{\lvert +3/2, m_I \rangle \leftrightarrow \lvert +1/2, m_I+1 \rangle} - H_{\lvert +3/2, m_I+1 \rangle \leftrightarrow \lvert +1/2, m_I \rangle}$	
m_I	Expt. (G)	Theor. (G)
$-\frac{5}{2}$	199.8	197.2
$-\frac{3}{2}$	205.1	202.7
$-\frac{1}{2}$	211.6	209.2
$+\frac{1}{2}$	218.1	215.8
$+\frac{3}{2}$	225.0	222.6

TABLE VIII. Observed and calculated doublet separations of forbidden transitions in Mn^{2+}:$ZnZrF_6 \cdot 6H_2O$. For $\Delta m_I = \pm 1$ in the $M_s = +\frac{3}{2} \leftrightarrow \frac{5}{2}$ fine-structure transition.

	$H_{\lvert +5/2, m_I \rangle \leftrightarrow \lvert +3/2, m_I+1 \rangle} - H_{\lvert +5/2, m_I+1 \rangle \leftrightarrow \lvert +3/2, m_I \rangle}$	
m_I	Expt. (G)	Theor. (G)
$-\frac{5}{2}$	361.7	360.2
$-\frac{3}{2}$	372.4	369.3
$-\frac{1}{2}$	381.3	378.8
$+\frac{1}{2}$	381.5	388.5
$+\frac{3}{2}$	401.2	398.5

TABLE IX. Observed and calculated doublet separations of forbidden transitions in Mn^{2+}:$CoZrF_6 \cdot 6H_2O$. For $\Delta m = \pm 1$ in the $M_s = -\frac{1}{2} \leftrightarrow +\frac{1}{2}$ fine-structure transition. The magnetic field H, makes an angle of 10° with c axis ($\nu = 9.246$ GHz, $T = 295$ K, $\theta = 10$).

	$H_{\lvert -1/2, m_I \rangle \leftrightarrow \lvert +1/2, m_I+1 \rangle} - H_{\lvert -1/2, m_I+1 \rangle \leftrightarrow \lvert +1/2, m_I \rangle}$	
m_I	Expt. (G)	Theor. (G)
$-\frac{5}{2}$	18.0	18.2
$-\frac{3}{2}$	21.0	21.4
$-\frac{1}{2}$	25.5	24.6
$+\frac{1}{2}$	28.5	27.8
$+\frac{3}{2}$	31.8	31.0

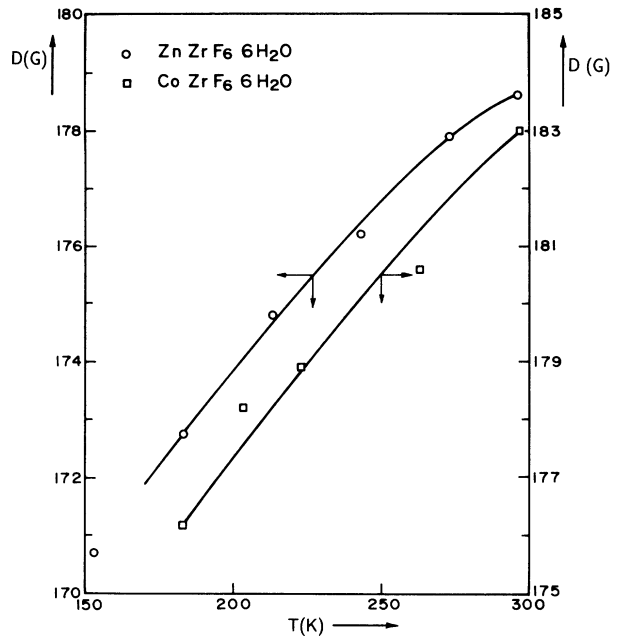

FIG. 5. Variation of zero-field splitting (ZFS) parameter, D, with temperature for Mn^2 in $ZnZrF_6 \cdot 6H_2O$ and $CoZrF_6 \cdot 6H_2O$.

D. Host spin-lattice relaxation in $CoZrF_6 \cdot 6H_2O$

Observation of resolved Mn^{2+} spectrum at room temperature in the paramagnetic $CoZrF_6 \cdot 6H_2O$ can be explained invoking a narrowing mechanism called the "host spin-lattice relaxation narrowing" mechanism, proposed by Mitsuma.[25] The fast spin-lattice relaxation of Co^{2+} ions leads to an appreciable averaging of the spin-spin interaction which is dipolar in nature. This results in the observed narrowing.

The host spin-lattice relaxation time T_1 is given by the expression[24,27]

$$T_1 = (3/20)(h/g_h\beta)(\Delta B_{pp}/B^2_{dip}) , \quad (6)$$

where $B^2_{dip} = 5.1(g_h\beta n)^2 S_h(S_h+1)$, ΔB_{pp} is the Mn peak-to-peak linewidth, g_h is the host g value, S_h is the host effective spin, β is the Bohr magneton, h is the Planck's constant, and n is the number of host ions per unit volume, which can be calculated from the crystallographic data.[15,16] Using this expression, T_1 for Co^{2+} at room temperature has been calculated in various lattices (Table X). In this calculation the data available for $CoSiF_6 \cdot 6H_2O$ were used. T_1 for the Co^{2+} ion in $CoZrF_6 \cdot 6H_2O$ at different temperatures is given in Table XI.

TABLE X. Spin-lattice relaxation time T_1 of Co^{2+} in some salts at room temperature.

System	T_1 10^{-12} s	Ref.
$CoZrF_6 \cdot 6H_2O$	3.8	This work
$CoTiF_6 \cdot 6H_2O$	0.6	11
$CoSiF_6 \cdot 6H_2O$	7.5	9
$CoSnF_6 \cdot 6H_2O$	3.9	12
$CoNbOF_5 \cdot 6H_2O$	0.7	24
$CoSO_4 \cdot 7H_2O$	11.0	26
$Co(NH_4)So_4 \cdot 6H_2O$	20.0	27
$CoK_2SO_4 \cdot 6H_2O$	10.0	28
$CoRb_2(SeO_4)_2 \cdot 6H_2O$	2.0	29
$CoCs_2(SeO_4)_2 \cdot 6H_2O$	1.78	29
$CO(CH_3COO)_2 \cdot 4H_2O$	9.1	30

DISCUSSION

Forbidden hyperfine lines

The large Q' value required to achieve an agreement with the observed separation leads us to believe that quadrupole coupling is sensitive to the immediate ligand field around the Mn^{2+} ion. Apart from the six water molecules which are arranged in a trigonally distorted octahedron around each Zn^{2+} ion, the six fluorines in the $(ZrF_6)^{4-}$ octahedron are hydrogen bonded to the protons of the water molecules. The bulky Zr atom hinders any rotation of the $(ZrF_6)^{4-}$ octahedron. This results in a steady electric-field gradient (EFG) at the oxygens of the water octahedron. This, most probably, is the reason for the relatively large Q' value that is required to explain the forbidden transitions within the hyperfine sextets corresponding to $M_s = \pm 3/2 \leftrightarrow \pm 5/2$ fine-structure transitions.

Phase transitions

The isomorphous fluosilicates and fluotitanates show structural phase transitions between 300–77 K, whereas fluostannates and fluozirconates do not exhibit such transitions. The relatively low atomic weights of Si (28.09)

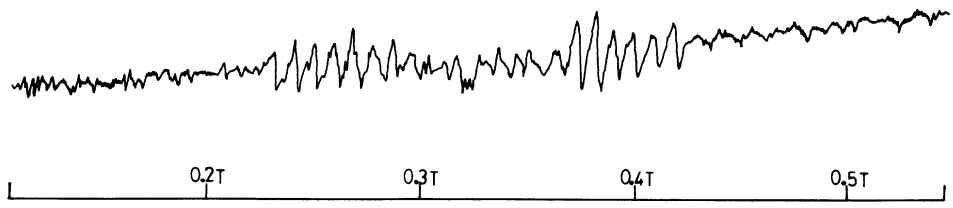

FIG. 6. EPR spectrum of Mn^{2+}:$CoZrF_6 \cdot 6H_2O$ at 193 K (ν=9.023 GHz).

TABLE XI. Temperature variation of spin-lattice relaxation time T_1 of Co^{2+} ion in $CoZrF_6 \cdot 6H_2O$.

Temperature (K)	T_1 (10^{-12} s)
183	9.5
203	6.3
223	5.1
243	4.4
263	3.9
295	3.8
313	3.5
343	2.4

and Ti (47.9) are favorable from the energy point of view for the rotation of the fluorine octahedron. In contrast, Zr (91.22) and Sn (118.67), being heavier, hinder the rotation. However, it is quite likely that at elevated temperatures, an onset of rotation of the fluorine octahedra could considerably reduce the ZFS. Such a dynamic behavior has been observed[14] in Mn^{2+}-doped $CaSnCl_6 \cdot 6H_2O$, where the transition from the trigonal to cubic phase was reported to occur at 413 K. This resulted in an isotropic sextet, indicating a ZFS $< A$, as against the value of 176 G ($\approx 2A$) observed at 293 K.

The fact that DSC shows a clear heat anomaly for the Zn as well as Co fluozirconate and the EPR spectra do not indicate any change can be interpreted as a change in the space group within the same point group, thus leaving the point symmetry unaltered. A recently reported[31] example of this is the phase transition at $T_c/K = 391$ in $[(CH_3)_4NCdBr_3]$.

Spin-lattice relaxation and exchange phenomena

The T_1 value observed for Co^{2+} in $CoZrF_6 \cdot 6H_2O$ is 3.79 (10^{-12} s), which is of the same order as reported for several cobalt complexes. The intensities of the hyperfine sextets corresponding to the five fine-structure transitions do not agree with the predicted ratio of 5:8:9:8:5. In addition, the whole spectrum was found to be shifted to the low-field side, indicating a departure of the g value (2.023) in the cobalt lattice from that in the Zn analog (1.996). It is quite possible that the intensity of the central sextet is considerably less than the predicted value, due to a possible overlap of the energy levels of Co^{2+} and Mn^{2+}. Francis and a Culvahouse[32] report a very broad line (nearly 1500 G) at $T/K = 4.2$. A further broadening of this absorption at higher temperature would therefore lead to the modulation of the predicted Mn^{2+} line intensities. Further, when the magnetic field is perpendicular to the c axis, the tail part of the broad absorption is found to shift to the high-field side,[32] thereby decreasing the overlap with the Mn^{2+} spectrum. Consequently, for $H \| c$ axis, the intensity of various hyperfine sextets, allowing for the overlap due to $D \approx 2A$, was closer to the predicted values as seen in Fig. 3(c).

In their magnetic studies on $CoSiF_6 \cdot 6H_2O$, Majumdar and Datta[33] reported large magnetic anisotropy in the plane containing the c axis, with the maximum along the c axis. The minimum, in a direction perpendicular to the c axis, was very close to the diamagnetic value observed in the isostructural diamagnetic zinc analog. Therefore along the c axis the modulation field due to the Co^{2+} ions is a maximum, while it is negligible in a perpendicular direction. This could also play a role in the observed intensities along and perpendicular to the c axis.

The departure of g in Mn^{2+}:$CoZrF_6 \cdot 6H_2O$ from that in the zinc analog, viz., 0.027 is due to the Co^{2+}-Mn^{2+} exchange. Whether this interaction is ferromagnetic or antiferromagnetic can be determined by evaluating the sign of J, the exchange interaction. Cobalt being a Kramers ion, the molecular-field approach of St. John and Myers[34] and Rubins and Drumheller[35] cannot be used. Hence more theoretical and experimental work, particularly concentration-dependent studies on Mn-Co systems, needs to be carried out for better understanding of the nature and strength of Co-Mn interaction.

ACKNOWLEDGMENTS

We would like to thank Professor K. Rama Reddy, Head, Department of Physics, Osmania University, for encouragement. We also thank K. Balarama Murty and N. Saratchandran of Nuclear Fuel Complex, Hyderabad, for providing us with high-purity zirconium oxide. We thank C.I.L., University of Hyderabad, for extending their EPR spectrometer facilities.

APPENDIX

Using third-order perturbation theory the following expressions have been obtained for the doublet separations of the forbidden hyperfine transitions within the various fine-structure transitions.

$M_s = +(1/2) \leftrightarrow -(1/2)$:

$\Delta m_I = \pm 1$ transitions:

$$\Delta H = H_{|1/2,m_I+1\rangle \leftrightarrow |-1/2,m_I\rangle} - H_{|1/2,m_I\rangle \leftrightarrow |-1/2,m_I+1\rangle}$$
$$= (17A^2/2H_0) + 2(\gamma\beta_N/g\beta)H_0 - (2m_I+1)[2P - (8A^2\sigma/H_0^2) + (25/2)(A^3/H_0^2) + (\gamma\beta_N/g\beta)A] . \quad \text{(A1)}$$

$\Delta m_I = \pm 2$ transitions:

$$\Delta H = H_{|1/2,m_I+1\rangle \leftrightarrow |-1/2,m_I-1\rangle} - H_{|1/2,m_I-1\rangle \leftrightarrow |-1/2,m_I+1\rangle}$$
$$= (17A^2/H_0) + 4(\gamma\beta_N/g\beta)H_0 - 2m_I[4P + (16A^2\sigma/H_0^2)(25A^3/H_0^2) + 2(\gamma\beta_N/g_\beta)A] . \quad \text{(A2)}$$

$M_s=+(3/2)\leftrightarrow+(1/2)$:
$\Delta m_I=\pm1$ transitions:

$$\Delta H=H_{|3/2,m_I+1\rangle\leftrightarrow|1/2,m_I\rangle}-H_{|3/2,m_I\rangle\leftrightarrow|1/2,m_I+1\rangle}$$
$$=-2A+2(\gamma\beta_N/g\beta)H_0-2P(2m_I+1)-(\lambda^2/H_0^2)(256/3)A$$
$$+(\rho^2/H_0^2)52A+(A^2/H_0)(2m_I+17/2)+(A^2\sigma/H_0^2)(14m_I+9)-(A^3/H_0^2)(m_I^2+19m_I-51/4)\ . \quad \text{(A3)}$$

$M_s=+(5/2)\leftrightarrow+(3/2)$:
$\Delta m_I=\pm1$ transitions:

$$\Delta H=H_{|5/2,m_I+1\rangle\leftrightarrow|3/2,m_I\rangle}-H_{|5/2,m_I\rangle\leftrightarrow|3/2,m_I+1\rangle}$$
$$=-4A+2(\gamma\beta_N/g\beta)H_0-2P(2m_I+1)-(\lambda^2/H_0^2)(40/3)A$$
$$+(56A)(\rho^2/H_0^2)+(A^2/H_0)(4m_I+13/2)+(A^2\sigma/H_0^2)(8m_I+8)-(A^3/H_0^2)(2m_I^2-m_I-33)\ . \quad \text{(A4)}$$

$M_s=-(3/2)\leftrightarrow-(1/2)$:
$\Delta m_I=\pm1$ transitions:

$$\Delta H=H_{|-1/2,m_I+1\rangle\leftrightarrow|-3/2,m_I\rangle}-H_{|-1/2,m_I\rangle\leftrightarrow|-3/2,m_I+1\rangle}$$
$$=-2A-2(\gamma\beta_N/g\beta)H_0+2P(2m_I+1)-(\lambda^2/H_0^2)(256/3)A$$
$$+(52A)(\rho^2/H_0^2)+(A^2/H_0)(2m_I-13/2)-(A^2\sigma/H_0^2)(14m_I+5)-(A^3/H_0^2)(m_I^2-17m_I-123/4)\ . \quad \text{(A5)}$$

$M_s=-(5/2)\leftrightarrow-(3/2)$:
$\Delta m_I=\pm1$ transitions:

$$\Delta H=H_{|-3/2,m_I+1\rangle\leftrightarrow|-5/2,m_I\rangle}-H_{|-3/2,m_I\rangle\leftrightarrow|-5/2,m_I+1\rangle}$$
$$=-4A-2(\gamma\beta_N/g\beta)H_0+2P(2m_I+1)-(\lambda^2/H_0^2)(40/3)A$$
$$+(56A)(\rho^2/H_0^2)+(A^2/H_0)(4m_I-5/2)-(A^2\sigma/H_0^2)(18m_I)-(A^3/H_0^2)(2m_I^2+5m_I-30)\ . \quad \text{(A6)}$$

To obtain the above expressions, H in the denominators has been approximated by the corresponding first-order expressions and the spin-Hamiltonian parameters are divided by $g\beta$. For example, H in the denominators of expressions for

$$H_{|1/2,m_I+1\rangle\leftrightarrow|-1/2,m_I\rangle} \quad \text{and} \quad H_{|1/2,m_I\rangle\leftrightarrow|-1/2,m_I+1\rangle}$$

have been approximated by $H_0-(A/2)(2m_I+1)$, where $H_0=(h\nu/g\beta)$.

[1]B. Bleaney and D. J. F. Ingram, Proc. R. Soc. London, Ser. A **205**, 336 (1951).
[2]E. Friedman and W. Low, Phys. Rev. **120**, 404 (1960).
[3]D. K. De, R. S. Rubins, and T. D. Black, Phys. Rev. B **29**, 71 (1984).
[4]R. S. Rubins and K. K. Kwee, J. Chem. Phys. **66**, 3948 (1977).
[5]R. Hrabanski, Solid State Commun. **64**, 117 (1987).
[6]R. Hrabanski, Spectrochim. Acta **44A**, 647 (1988).
[7]R. Hrabanski, Spectrochim. Acta **48A**, 631 (1992).
[8]B. Bleaney and R. S. Rubins, Phys. Rev. **112**, 103 (1961).
[9]G. Jayaram and G. S. Sastry, Chem. Phys. Lett. **77**, 314 (1981).
[10]G. Jayaram and G. S. Sastry, Chem. Phys. Lett. **97**, 431 (1983).
[11]G. Jayaram, Z. Naturforsch. (to be published).
[12]G. Jayaram (unpublished).
[13]A. M. Ziatdinov, M. M. Zaripov, Yu. V. Yablokov, and R. L. Davidovich, Phys. Status Solidi B **78**, K69 (1976).
[14]T. Kitazume, M. Sekizaki, and M. Suhara, J. Mol. Struct. **58**, 161 (1980).
[15]R. L. Davidovich, T. F. Levchishina, T. A. Kaidalova, and Yu. A. Buslaev, Izv. Akad. Nauk. SSSR Neorg. Mater. **6**, 495 (1970).
[16]M. M. Zaripov, A. M. Ziatdinov, Yu. V. Yablokov, R. L. Davidovich, and T. F. Levchishina, Fiz. Tverd. Tela (Leningrad) **17**, 1164 (1975) [Sov. Phys. Solid State **17**, 745 (1975)].
[17]B. Bleaney and R. S. Trenam, Proc. R. Soc. London, Ser. A **223**, 1 (1954).
[18]J. Schneider and S. R. Sircar, Z. Naturforsch. **17a**, 651 (1962).
[19]F. Waldner, Helv. Phys. Acta **35**, 756 (1962).
[20]T. Takeda, J. Phys. Soc. Jpn. **23**, 1314 (1967).
[21]H. W. Dewijn and R. F. van Balderen, J. Chem. Phys. **46**, 1381 (1967), and references therein.
[22]Yu. V. Yablokov, M. M. Zaripov, A. M. Ziatdinov, and R. L. Davidovich, Chem. Phys. Lett. **48**, 443 (1977).
[23]S. K. Misra and M. Jalochowski, Physica B **119**, 295 (1983).
[24]R. Murugesan and S. Subramanian, J. Magn. Reson. **57**, 385 (1984).
[25]T. Mitsuma, J. Phys. Soc. Jpn. **17**, 128 (1962).

[26]R. S. Saraswat and G. C. Upreti, Phys. Status Solidi B **87**, K39 (1978).
[27]R. S. Saraswat and G. C. Upreti, J. Chem. Phys. **67**, 5428 (1977).
[28]V. K. Jain, J. Magn. Reson. **64**, 512 (1985).
[29]V. K. Jain and S. K. Yadav, Solid State Commun. **59**, 313 (1986).
[30]G. C. Upreti and R. S. Saraswat, Magn. Reson. Rev. **7**, 215 (1982).
[31]T. Asahi, K. Hasebe, and K. Gesi, Acta Crystallogr. C **47**, 1208 (1991).
[32]L. L. Francis and J. W. Culvahouse, J. Chem. Phys. **66**, 1089 (1977).
[33]M. Majumdar and S. K. Datta, J. Chem. Phys. **42**, 418 (1965).
[34]M. R. St. John and R. J. Myers, Phys. Rev. B **13**, 1006 (1976); M. R. St. John, Ph.D. thesis, University of California, Berkeley.
[35]R. S. Rubins and J. E. Drumheller, Phys. Rev. B **32**, 7098 (1985).